Characterization of the vaccinia virus D10 decapping enzyme provides evidence for a two-metal-ion mechanism

Article *in* Biochemical Journal · March 2009

DOI: 10.1042/BJ20082296 · Source: PubMed

3 authors, including:

Marie Soulière

14 PUBLICATIONS **644** CITATIONS

SEE PROFILE

Jean-Pierre Perreault

Université de Sherbrooke

265 PUBLICATIONS **5,743** CITATIONS

SEE PROFILE

BJ www.biochemj.org

BJ Cell

Biochem. J. (2009) **420**, 27–35 (Printed in Great Britain) doi:10.1042/BJ20082296

online data

27

Characterization of the vaccinia virus D10 decapping enzyme provides evidence for a two-metal-ion mechanism

Marie F. SOULIÈRE, Jean-Pierre PERREAULT and Martin BISAILLON[1]

RNA Group/Groupe ARN, Département de Biochimie, Faculté de Médecine et des Sciences de la Santé, Université de Sherbrooke, Sherbrooke, QC, Canada, J1H 5N4

Decapping enzymes are required for the removal of the 5′-end cap of mRNAs. These enzymes exhibit a specific hydrolase activity, resulting in cleavage between the α- and β-phosphates of the ^{m7}GpppN cap to generate both ^{m7}GDP and monophosphorylated RNA products. Decapping enzymes have been found in humans, plants and yeasts, and have been discovered more recently in vaccinia virus (D10 protein). Although experimental evidences are lacking, three-metal- and two-metal-ion mechanisms have been proposed so far for the decapping enzymes. In the present study, we performed a biochemical characterization of the interaction of bivalent cations with the vaccinia virus D10 protein. Synergistic activation of the enzyme was observed in the presence of Mg^{2+} and Mn^{2+} ions, suggesting the existence of two metal-ion-binding sites on the D10 protein. Moreover, dual-ligand titration experiments using fluorescence spectroscopy demonstrated the presence of two metal-ion-binding sites on the enzyme. A three-dimensional structural model of the active site of the enzyme was generated which highlighted the importance of three glutamate residues involved in the co-ordination of two metal ions and a water molecule. Mutational analyses confirmed the role of two glutamate residues for the binding of metal ions. We demonstrate that one metal ion is co-ordinated by Glu^{132}, while the second metal ion is co-ordinated by Glu^{145}. Taken together, these results support the proposed two-metal-ion mechanistic model for the D10 decapping enzyme.

Key words: decapping enzyme, enzyme mechanism, mRNA metabolism, Nudix motif, structural modelling, vaccinia virus.

INTRODUCTION

mRNA decay occurs in cytoplasmic regions of the cells, named P-bodies (processing bodies), consisting of many enzymes involved in mRNA turnover, including decapping enzymes [1,2]. The latter are required for the removal of the 5′-end cap of mRNAs. The human, plant and yeast decapping enzymes (Dcp2) exhibit a specific hydrolase activity, resulting in cleavage between the α- and β-phosphates of the ^{m7}GpppN cap to generate both ^{m7}GDP and monophosphorylated RNA products, whereas the scavenger decapping proteins (DcpS) cleave between the β- and γ-phosphates of the cap structure [3–7]. The remaining mono- or di-phosphorylated mRNAs are then subjected to 5′→3′ exonucleolytic degradation. Decapping enzymes involved in the turnover of mRNAs have been found in many species throughout the eukaryotic tree [3,6]. Moreover, it was shown previously that the vaccinia virus also encodes decapping enzymes, the D9 and D10 proteins (D9p and D10p) [8–10]. The discovery that mammalian viruses can harbour decapping enzymes has important implications for the control of viral and cellular gene expression. It has been suggested that the presence of decapping enzymes in vaccinia virus is likely to be required to eliminate competing host mRNAs and to allow stage-specific synthesis of viral proteins [8].

D10p is expressed during late viral transcription, and deletion of the D10 gene was shown to produce a 10-fold reduction of the infectious viral particle formation [11]. Furthermore, previous studies demonstrated the ability of D10p to hydrolyse capped RNA of at least 24 nt in length to release an ^{m7}GDP product in the presence of bivalent cations [8]. The decapping activity was inhibited by either methylated cap analogues or uncapped RNA, suggesting recognition through both cap and RNA chain. D9p possesses 25 % identity with D10p, but is differentially expressed during early viral transcription [9]. D9p demonstrated the same requirements as D10p for its decapping activity. Results from inhibition studies revealed that the decapping activity of D9p is strongly reduced by uncapped RNA, whereas methylated nucleotides have a higher inhibitory effect on D10p. These data suggest a differential binding of the two enzymes to their substrates [10].

Both D10p and D9p belong to a superfamily of hydrolases characterized by a consensus Nudix sequence [12,13]. This motif has been shown to be essential for the decapping activity of Dcp2 enzymes [3,14]. The Nudix hydrolase superfamily is widespread among eukaryotes, bacteria, archaea and viruses, and includes enzymes which cleave nucleoside diphosphates linked to other moieties. This family encompasses enzymes such as Ap_4A (adenosine 5′-tetraphospho-5′-adenosine pyrophosphatase), MutT pyrophosphohydrolase, GDPMH (GDP-mannose mannosyl hydrolase) and decapping enzymes. The catalytic activity of the Nudix hydrolase enzymes is strictly dependent on the conserved 23-amino-acid Nudix motif, i.e. $GX_5EX_7REUXEEXGU$, where U is a bulky hydrophobic amino acid and X is any amino acid [14,15]. The Nudix motif forms a loop–α-helix–loop secondary structure, which is involved in bivalent cation interaction. However, even with this high conservation of the catalytic motif, the Nudix hydrolases exhibit diverse enzymatic mechanisms [14,16,17]. For example, MutT pyrophosphohydrolase utilizes two metal ions for its mechanism, with one ion interacting directly with the enzyme and the second co-ordinating the β- and γ-phosphates of the NTP substrate. However, Ap_4A has been shown to require three bivalent cations, with the third ion joining

Abbreviations used: Ap_4A, adenosine 5′-tetraphospho-5′-adenosine pyrophosphatase; Dcp, decapping enzyme; AtDcp2p, *Arabadopsis thaliana* Dcp2 protein; hDcp2p, human Dcp2 protein; SpDcp2p, *Schizosaccharomyces pombe* Dcp2 protein; DTT, dithiothreitol; Ni-NTA, Ni^{2+}-nitrilotriacetate; P-body, processing body.

[1] To whom correspondence should be addressed (email Martin.Bisaillon@USherbrooke.ca).

the complex to support co-ordination of the attacking nucleophile [18]. The precise mechanism used by the decapping enzymes has not yet been demonstrated. It has been suggested that these enzymes might utilize a three-bivalent-cation mechanism since the catalytic reaction is similar to the ADP-ribose pyrophosphatase, another Nudix hydrolase which harbours a three-metal-ion interaction in its crystal structure [19]. More recently, mutational analysis of AtDcp2p (*Arabidopsis thaliana* Dcp2 protein) led to the proposal of a two-metal-ion model for this enzyme [4].

The present study proposes a biochemical characterization of the interaction of bivalent cations with the vaccinia virus D10p. We investigated the ability of the enzyme to interact with both Mg^{2+} and Mn^{2+} ions and provide evidence for a two-metal-ion mechanism. Moreover, the generation of specific glutamate mutants of D10p outlined the residues involved in the interaction with the two metal ions.

MATERIALS AND METHODS

D10 expression and purification

A plasmid for the expression of a full-length D10 protein (248 amino acids) was generated by inserting the vaccinia D10R gene between the NdeI and HindIII cloning sites of the pET28a expression plasmid (Novagen). In this context, the D10 protein is fused in-frame with a N-terminal peptide containing six tandem histidine residues, and expression of the His_6-tagged protein is driven by a T7 RNA polymerase promoter. The resulting recombinant plasmid (pET-D10) was transformed into *Escherichia coli* BL21(DE3) cells and a 1 litre culture of *E. coli* BL21(DE3)/pET-D10 was grown at 37 °C in Luria–Bertani medium containing 0.1 mg/ml ampicillin until the D_{600} reached 0.5. The culture was adjusted to 0.4 mM isopropyl β-D-thiogalactoside and 2 % ethanol, and the incubation continued at 18 °C for 20 h. The cells were then harvested by centrifugation at 3500 ***g*** for 15 min, and the pellets were stored at − 80 °C. All subsequent procedures were performed at 4 °C. Thawed bacteria pellets were resuspended in 50 ml of lysis buffer A (50 mM Tris/HCl, pH 7.5, 150 mM NaCl and 10 % sucrose), and cell lysis was achieved by adding lysozyme and Triton X-100 to final concentrations of 50 μg/ml and 0.1 % respectively. The lysates were sonicated to reduce viscosity, and any insoluble material was removed by centrifugation at 13 000 rev./min for 45 min at 4 °C (Sorvall SLA1500 rotor). The soluble extract was applied to a 2 ml column of Ni-NTA (Ni^{2+}-nitrilotriacetic acid)–agarose (Qiagen) that had been equilibrated with buffer A containing 0.1 % Triton X-100. The column was washed with the same buffer and then eluted stepwise with buffer B (50 mM Tris/HCl, pH 8.0, 100 mM NaCl and 10 % glycerol) containing 50, 100, 200, 500 or 1000 mM imidazole. The polypeptide composition of the column fractions was monitored by SDS/PAGE (12 % gels). The recombinant D10 protein was retained on the column and recovered in the 500 and 1000 mM imidazole eluates. Following a 4 h dialysis against buffer C [50 mM Tris/HCl, pH 8.0, 50 mM NaCl, 2 mM dithiothreitol (DTT) and 10 % glycerol], the protein concentration was determined by the Bio-Rad dye-binding method using BSA as the standard. D10p E132A, E141A and E145A mutants were also cloned and expressed using this method.

7-Methyl-capped RNA synthesis

An RNA substrate of 81 nt was synthesized using a pair of complementary oligonucleotides including a T7 RNA promoter followed by the sequence of the substrate. Following transcription, the RNA substrate was purified on a denaturing 8 % polyacrylamide gel and visualized by UV-shadowing. The corresponding band was excised, and then eluted from the gel by an overnight incubation in 0.1 % SDS/0.5 M ammonium acetate. The RNA was then precipitated with propan-2-ol, and the pellets were resuspended in nanopure water. The purified 5′-triphosphorylated 81-nt RNA was processed further for 1 h in capping buffer (50 mM Tris/HCl, pH 7.5, 5 mM DTT and 20 mM $MgCl_2$) using the vaccinia virus RNA 5′-triphosphatase/RNA 5′-guanylyltransferase D1R to first obtain a diphosphorylated 5′-end. Afterwards, 1 μM [α-^{32}P]GTP was added to the reaction mixture to allow the radiolabelled capping of the diphosphorylated RNA for 1 h. This capped RNA was again subjected to a phenol/chloroform purification and propan-2-ol precipitation. The resuspended capped RNA was methylated using the *Saccharomyces cerevisiae* guanine-7-methyltransferase (Abd1) in methylation buffer (50 mM Tris/HCl, pH 7.5, 5 mM DTT and 40 mM NaCl) with 2 μM adenosylmethionine for 1 h. This 7-methyl-capped RNA was again purified on an 8 % polyacrylamide gel, excised and precipitated. The RNA substrate was then quantified by spectrophotometry and stored at − 20 °C.

Decapping assays

Reaction mixtures (20 μl) containing 10 mM Tris/HCl (pH 7.5), 100 mM potassium acetate, 1 mM DTT, 0.5 μM γ-phosphate-labelled 7-methyl-capped RNA substrate and 1 μM purified D10 protein were incubated for 90 min at 37 °C in the presence of various metal ion concentrations. The reactions were quenched by adding 2 μl of 0.5 M EDTA. Aliquots of the mixtures were applied to a polyethyleneimine–cellulose TLC plate, which was developed with 0.5 mM LiCl and 1 M methanoic (formic) acid. The release of γ-phosphate-labelled ^{m7}GDP was revealed by autoradiography with a phosphoimager (Amersham Biosciences) and quantified using ImageQuant 5.0 (Molecular Dynamics). In the case of NaF inhibition assays, the reactions were stopped after 1 h. Reaction mixtures where then treated as stated above. Furthermore, for the synergy assays, Mg^{2+} and Mn^{2+} ions were added separately or simultaneously to reaction mixtures, which were incubated for 1 h at 37 °C and treated further as stated above. Experiments were performed a minimum of three times separately.

Fluorescence measurements

Fluorescence was measured using an Hitachi F-2500 fluorescence spectrophotometer. Background emission was eliminated by subtracting the signal from either buffer alone or buffer containing the appropriate quantity of substrate. The extent to which ligands bind to the D10 protein was determined by monitoring the fluorescence emission of a fixed concentration of proteins and titrating with a given ligand. The binding can be described by eqn (1):

$$K_d = \frac{[\text{D10p}][\text{ligand}]}{[\text{D10p} \cdot \text{ligand}]} \quad (1)$$

where K_d is the apparent dissociation constant, [D10p] is the concentration of the protein, [D10p·ligand] is the concentration of complexed protein, and [ligand] is the concentration of unbound ligand in solution. The proportion of ligand-bound protein, as described by eqn (1), is related to measured fluorescence emission intensity by eqn (2):

$$\Delta F / \Delta F_{max} = \frac{[\text{D10p} \cdot \text{ligand}]}{[\text{D10p}]_{tot}} \quad (2)$$

where ΔF is the magnitude of the difference between the observed fluorescence intensity at a given concentration of ligand and the fluorescence intensity in the absence of ligand, ΔF_{max} is the difference at infinite [ligand], and $[D10p]_{tot}$ is the total protein concentration.

If the total ligand concentration, $[ligand]_{tot}$, is in large molar excess relative to $[D10p]_{tot}$, then it can be assumed that [ligand] is approximately equal to $[ligand]_{tot}$. Eqns (1) and (2) can then be combined to give eqn (3):

$$\Delta F/\Delta F_{max} = \frac{[ligand]_{tot}}{K_d + [ligand]_{tot}} \quad (3)$$

The K_d values were determined from a non-linear least-square regression analysis of titration data by using eqn (3). Fluorescence experiments were performed a minimum of three times separately.

Analysis of competitive metal ion binding

Analysis of the effect of a fixed concentration of one metal ion ligand (ion_a) on the binding of a second ion ligand (ion_b) was performed in a manner analogous to that reported previously for analysing the kinetics of a system in which two alternative substrates compete for the same enzyme-binding site [20]. The change in fluorescence (ΔF) observed upon titration of D10p with ion_a in the presence of a fixed concentration of competing substrate (ion_b) can be described by eqn (4):

$$\Delta F = \Delta F_{max(a)}\left(\frac{[ion_a]}{K_a}\right) + \Delta F_{max(b)}\left(\frac{[ion_b]}{K_b}\right) + \frac{[ion_a]}{K_a} + \frac{[ion_b]}{K_b} \quad (4)$$

where $\Delta F_{max(a)}$ and $\Delta F_{max(b)}$ are the changes in fluorescence produced at infinite concentrations of ion_a and ion_b respectively, and K_a and K_b are the apparent dissociation constants for ion_a and ion_b respectively. Eqn (4) was fitted to the simple ligand saturation isotherms for both ion_a and ion_b.

CD spectroscopy measurements

CD measurements were performed using a Jasco J-810 spectropolarimeter. The samples were analysed in quartz cells with pathlengths of 1 mm. Far-UV wavelength scans were recorded from 200 to 250 nm. The average of three wavelength scans is presented. The ellipticity results were expressed as mean residue ellipticity, in millidegrees (mdeg).

Homology modelling

The crystal structure of SpDcp2p (*Schizosaccharomyces pombe* Dcp2 protein) was used as a template to model the vaccinia virus D10 protein. The atomic co-ordinates were obtained from the Protein Data Bank file 2A6T. The predicted three-dimensional structure of the D10 protein active site was generated with the Deep View program [21].

RESULTS

Expression and decapping activity of D10p

A His_6-tagged version of the 248-amino-acid vaccinia virus D10p was expressed in *E. coli* and purified by Ni-NTA–agarose chromatography. SDS/PAGE analysis demonstrated that the 31 kDa recombinant D10p was the predominant polypeptide in the purified fraction (Figure 1A). Size-exclusion chromatography assays performed on the purified D10p to assess its possible homodimerization revealed a unique absorbance peak around 31 kDa, the expected molecular mass of a D10p monomer (results not shown).

The decapping activity of the purified protein was initially evaluated using a radiolabelled methyl-capped RNA substrate in the presence of increasing concentrations of Mn^{2+} ions (Figure 1B). The reactions products were then separated by TLC. As seen in Figure 1(B), only the ^{m7}GDP product and the initial capped ^{m7}Gppp-RNA substrate were detected, indicating that the reaction is specific and does not yield any other side product (Figure 1B). Decapping activity reached a maximum (>95 %) at a concentration of 5 mM for Mn^{2+} (Figures 1B and 1D).

We next sought to investigate the ability of Mg^{2+} ions to support the decapping activity of the vaccinia virus D10 protein. Once again, maximal hydrolysis was reached at a metal ion concentration of 5 mM (Figure 1C). However, under these conditions, only 45 % of the radiolabelled methyl-capped RNA substrate was hydrolysed by the enzyme (Figures 1C and 1D). This difference in catalysis is also reflected by the different pseudo-catalytic constants (k_{cat}') determined in the presence of the two metal ions (0.2 min^{-1} and 0.1 min^{-1} for Mn^{2+} and Mg^{2+} ions respectively).

Previous studies have demonstrated the high sensitivity of other Nudix hydrolases, such as Ap_4P and the coenzyme A hydrolase, to F^- ions, whereas AtDcp2p was only moderately affected under the same conditions [4,14,22]. The susceptibility of the recombinant D10p to inhibition by F^- ions was therefore tested. Similarly to AtDcp2p, D10p did not present any susceptibility to F^- ions in the presence of $MnCl_2$ or $MgCl_2$ (Figure 1E). This is also evident by the k_{cat}' values which remained identical upon incubation with 0.1 mM NaF (0.2 min^{-1} and 0.1 min^{-1} in the presence of Mn^{2+} and Mg^{2+} ions respectively). However, a moderate inhibition could be observed in the presence of $MgCl_2$ when the enzyme was incubated with a very high concentration of NaF (5 mM) (Figure 1E). These results demonstrate that the two decapping enzymes, D10p and AtDcp2p, share a similar lack of inhibition by F^- ions, which sets them apart from other Nudix hydrolase family members.

Interaction with bivalent cations

Fluorescence spectroscopy was used to monitor the interaction of metal ions to D10p. Using the intrinsic fluorescence of the sole tryptophan residue of the D10 protein (Trp^{43}), the enzyme was excited at a wavelength of 290 nm. The enzyme in standard buffer generated a fluorescence emission spectrum with a maximal peak at 336 nm (Figure 2A). Analysis of the molar intensity of the fluorescence emission of D10p revealed a linear change of 7.3 fluorescence intensity units/μM of protein over the range examined (Figure 2A, inset). This relatively small change can probably be attributed to small losses of proteins from solution through adhesion. All subsequent binding experiments were performed at a protein concentration of 1 μM, with the assumption that the binding equilibrium was not affected by the presence of aggregation equilibrium.

To evaluate the K_d for the interaction of metal ions with the recombinant D10p, various concentrations of either $MgCl_2$ or $MnCl_2$ were added to the purified enzyme and the fluorescence emission was monitored. A decrease in fluorescence intensity was observed when the protein was titrated with increasing amounts of Mg^{2+} or Mn^{2+} ions (Figure 2B, inset). No variation in fluorescence intensity was observed upon addition of Ca^{2+}, Na^+ or Li^+ ions to D10p, supporting the specificity of the binding observed

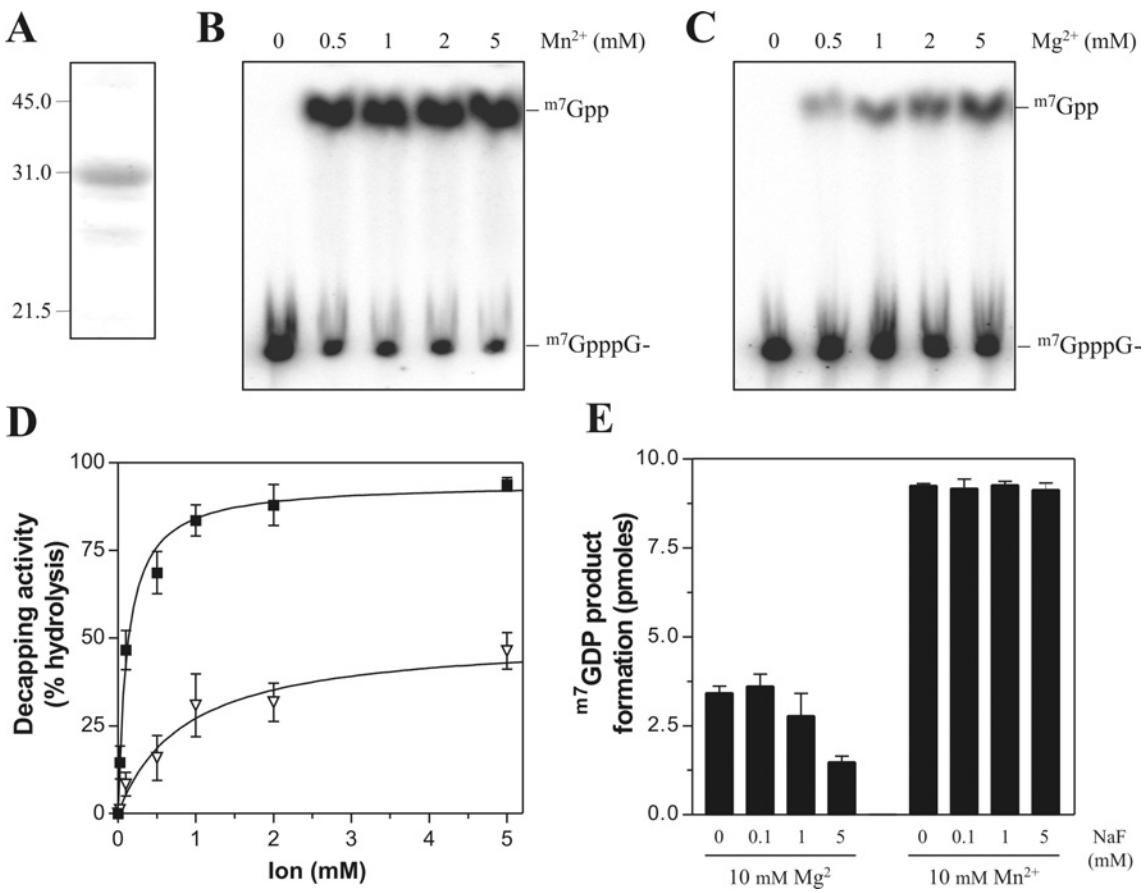

Figure 1 Expression and activity of the D10 protein

(**A**) An aliquot (0.5 μg) of the purified preparation of D10p was analysed by electrophoresis through a 12.5 % polyacrylamide gel containing 0.1 % SDS, and visualized by staining with Coomassie Blue dye. The positions and sizes in kDa of the molecular-mass standards are indicated on the left. (**B** and **C**) The enzyme (1 μM) and methyl-capped RNA substrate (0.5 μM) were incubated for 90 min at 37 °C with increasing concentrations of $MnCl_2$ (**B**) or $MgCl_2$ (**C**) in 10 mM Tris/HCl (pH 7.5), 100 mM potassium acetate, 5 mM $MgCl_2$ and 1 mM DTT buffer (decapping buffer). The reactions were stopped by the addition of EDTA to 50 mM. The products were analysed by TLC. An autoradiogram of the plate is shown. The positions of the unlabelled products, visualized under UV light, are indicated. (**D**) A saturation isotherm can be generated from these data by plotting the product formation as a function of either $MgCl_2$ (∇) or $MnCl_2$ (■) concentrations. Results are means ± S.E.M. of three replicates. (**E**) The effect of F^- ions on the activity of 1 μM D10p on 0.5 μM capped RNA substrate was observed by adding increasing concentrations of NaF (0–50 mM) to the reactions performed in the presence of 10 mM $MgCl_2$ or $MnCl_2$.

in the presence of Mg^{2+} or Mn^{2+} ions (see Supplementary Figure S1 at http://www.BiochemJ.org/bj/420/bj4200027add.htm). The binding data for Mg^{2+} and Mn^{2+} ions indicate that the enzyme displays similar affinity for both metal ions, as determined from the respective K_d and ΔG values (Figure 2B and Table 1). In order to confirm these results, we also evaluated the binding of Mn^{2+} and Mg^{2+} to D10p using CD. The molar ellipticity of the enzyme was monitored from 200 to 250 nm as a function of added Mg^{2+} or Mn^{2+} ions (Figure 2C). A plot of the ellipticity variation at 222 nm, representative of changes in α-helical structures, as a function of added bivalent cations is presented (Figure 2D). The estimated dissociation constants corroborate the results obtained in fluorescence spectroscopy experiments, with K_d values of 4.7 ± 1.7 mM for the binding of Mn^{2+} ions, and 2.1 ± 0.4 mM for the interaction of Mg^{2+} ions with D10p.

Analysis of Hill plots generated from the Mg^{2+} and Mn^{2+} fluorescence spectroscopy binding assays indicated a lack of co-operativity ($h = 0.9 \pm 0.3$) for the binding of both ions to D10p (see Supplementary Figure S2A at http://www.BiochemJ.org/bj/420/bj4200027add.htm). However, derivation of the binding data with the Scatchard equation yielded curves displaying the typical appearance of two-site binding plots, for both metal ions (Supplementary Figure S2B). These results suggest the presence of two metal-ion-binding sites on D10p with no discernable co-operativity between the two sites. The association rate of both ions to D10p was also evaluated by real-time fluorescence spectroscopy (Figure 2E). Both ions associate readily with the enzyme, as judged from the association rate values obtained for Mn^{2+} and Mg^{2+} binding to D10p (4.1 ± 0.4 and 3.7 ± 0.7 $mM^{-1} \cdot s^{-1}$ respectively).

With the difference in catalytic activity of D10p observed in the presence of Mg^{2+} or Mn^{2+} ions, and the differences in the binding of the two ions to the enzyme, we wondered whether the two metal ions bind to the same site on D10p. To answer this question, we performed competitive alternative ligand-binding experiments using fluorescence spectroscopy. The saturation isotherm determined for the binding of Mn^{2+} to D10p was compared with curves obtained in the presence of Mn^{2+} and either 1 or 5 mM Mg^{2+} (Figure 2F). We also performed the reverse experiment, where Mg^{2+} binding was competed with increasing Mn^{2+} concentrations (see Supplementary Figure S3 at http://www.BiochemJ.org/bj/420/bj4200027add.htm). Both results are in accordance with a model in which the binding of Mg^{2+} and Mn^{2+} is not mutually exclusive [23,24]. Instead, the addition of the second ion (Mg^{2+}) yields an additive variation in the fluorescence emitted by D10p already saturated with the first one. We conclude

Table 1 Bivalent cation dissociation constants (K_d) and Gibbs free energy (ΔG)

1 kcal = 4.184 kJ.

D10p	$K_{Mg^{2+}}$ (mM)	$K_{Mn^{2+}}$ (mM)	$\Delta G_{Mg^{2+}}$ (kcal/mol)	$\Delta G_{Mg^{2+}}$ (kcal/mol)
Wild-type	2.0 ± 0.6	4.2 ± 1.3	-3.7 ± 0.2	-3.4 ± 0.2
E132A	9.1 ± 2.2	7.6 ± 2.2	-2.8 ± 0.1	-2.9 ± 0.2
E141A	2.5 ± 0.8	9.0 ± 2.0	-3.6 ± 0.2	-2.8 ± 0.1
E145A	5.1 ± 2.1	25.9 ± 5.9	-3.2 ± 0.3	-2.2 ± 0.1

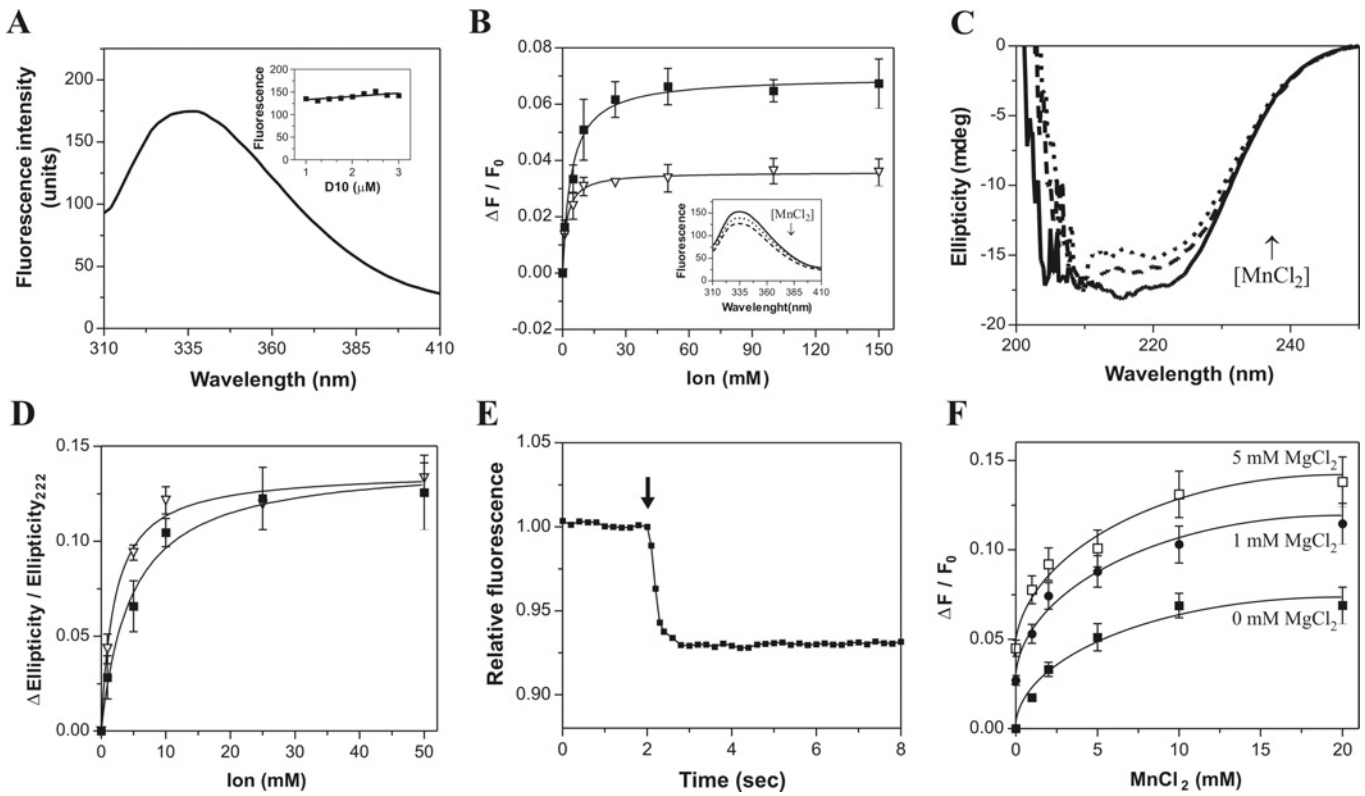

Figure 2 Titration of D10p with bivalent cations

(**A**) Fluorescence emission spectra of 1 μM D10p in decapping buffer. The inset shows the molar fluorescence of D10p where various concentrations of the purified protein were assayed. Emission was monitored at 339 nm, after excitation at 290 nm. (**B**) The effect of increasing amounts of $MnCl_2$ added to the enzyme on the fluorescence spectra is shown in the inset. The emission spectrum was scanned from 310 to 440 nm. A saturation isotherm can be generated from these data by plotting the change in fluorescence intensity at 339 nm as a function of added $MnCl_2$ (■). Results for $MgCl_2$ binding are also shown (∇). For both ions, results are means ± S.E.M. of three replicates. (**C**) D10p was titrated with increasing Mn^{2+} concentrations in decapping buffer, and the resulting conformational changes were monitored using CD. The far-UV (200–250 nm) spectra obtained for D10p alone or in the presence of 25 or 50 mM $MnCl_2$ are presented. (**D**) A saturation isotherm can be generated from these data by plotting the change in ellipticity at 222 nm as a function of added $MgCl_2$ (∇) or $MnCl_2$ (■). (**E**) Kinetic analysis of real-time binding of $MnCl_2$ to D10p. $MgCl_2$ (100 mM) was injected to the enzyme in decapping buffer, and emission was monitored for 20 s at 335 nm, after excitation at 290 nm. (**F**) Standard titration assays were performed using Mn^{2+} ions in the presence of increasing amounts of Mg^{2+} ions. The concentrations of Mg^{2+} ions used in these experiments were 0 (■), 1 (●) and 5 (□) mM.

that at least two metal-ion-binding sites are present on the enzyme.

Synergistic activation of D10p by metal ions

The previous results led us to suspect that D10p exploits a two-metal-ion mechanism for catalytic activity to occur. With the assumption that each site demonstrates a preference for either Mg^{2+} or Mn^{2+}, a mixture of suboptimal concentrations of each metal ion should produce a synergistic activation of the D10p activity. Such activation was observed using concentrations of 0.25 and 0.5 mM of each ion (Figure 3). In the presence of 0.25 mM $MgCl_2$, the addition of D10p resulted in the release of 0.11 ± 0.05 pmol of product, whereas 1.4 ± 0.5 pmol was generated in the presence of 0.25 mM $MnCl_2$. However, with 0.25 mM of both ions, 3.1 ± 0.2 pmol of product was released. The latter product formation equals to more than the sum of the products generated with each ion separately. Similar results were obtained using 0.5 mM $MgCl_2$ or $MnCl_2$. This synergistic activation of D10p is in agreement with a two-metal mechanism [25,26].

In order to emphasize that the previous results were specifically due to the presence of these two particular ions, and not of an ionic environment change generated by the addition of another bivalent cation in solution, the latter experiment was repeated in the presence of $CaCl_2$ and $CoCl_2$. Ca^{2+} ions could not support D10p activity and did not produce a synergistic activation of D10p in the presence of Mn^{2+} (Figure 3). The Co^{2+} ions, however,

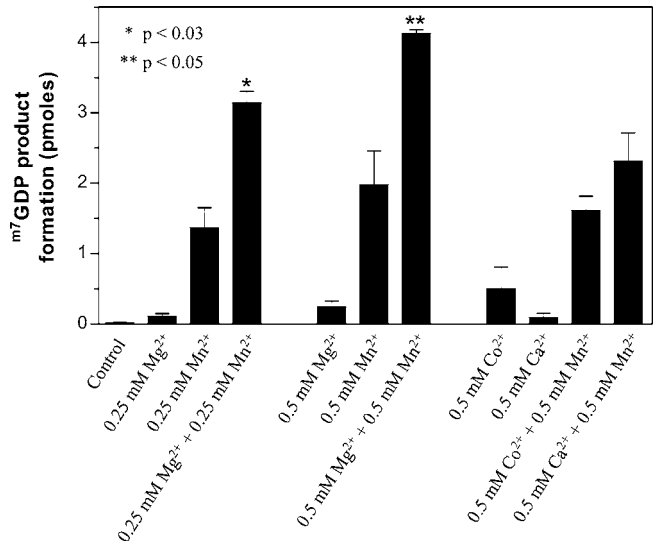

Figure 3 Synergistic activation of D10p

Reaction mixtures containing 1 μM D10p, 0.5 μM capped RNA substrate and various concentrations of metal ions, were incubated for 1 h at 37 °C. The products were analysed by TLC and quantified by autoradiography. Results are means $\pm$ S.E.M. of three replicates.

supported D10p catalytic activity, but also failed to demonstrate a synergistic effect on the enzyme when tested with Mn^{2+} ions (Figure 3). We therefore conclude that the synergistic activation of D10p by Mn^{2+} and Mg^{2+} is a specific effect, due to the presence of both ions and not to a modification of the ionic strength of the reaction mixture.

Modelling of the active site and mechanism of action

The Dcp2 proteins examined so far present three highly conserved domains required for different aspects of their activity. A main 109-amino-acid Nudix domain comprising the 23-amino-acid Nudix motif is required for the hydrolytic activity of the enzymes. This region is surrounded by two additional domains (a 38-amino-acid Box A and a 20-amino-acid Box B) [3,15]. Box A has been associated with the specificity of the hydrolytic activity of the enzyme in hDcp2p (human Dcp2 protein), whereas Box B is structured into an α-helix and appears to be required for the interaction with RNA. Analysis of the D10p amino acid sequence does not reveal a high homology with the Box A found in other decapping enzymes. Only four of the 14 absolutely conserved amino acids in yeast, plants and humans are found in D10p (Figure 4A) [6]. Moreover, the enzyme possesses only two of the four main amino acids conserved in the Box B of decapping enzymes (Figure 4A). However, structural modelling of the D10p region corresponding to the Box B suggests that it could still adopt an α-helical structure (results not shown). Interestingly,

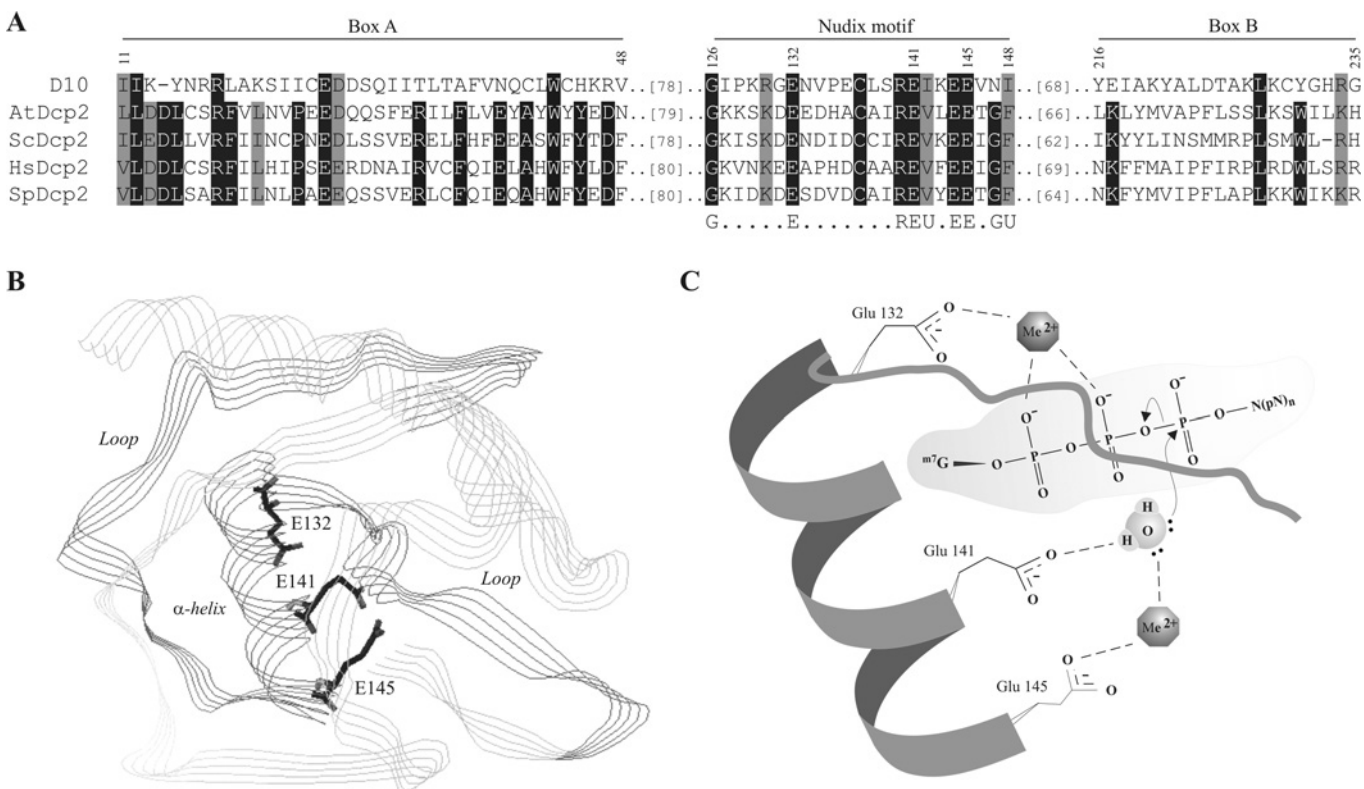

Figure 4 Sequence conservation within the Nudix motif of decapping enzymes and modelling of the D10 protein

(**A**) Alignments of amino acids 11–48, 126–148 and 216–235 respectively from the Box A, Nudix motif and Box B of the vaccinia virus D10 protein are presented with the corresponding motifs in AtDcp2, *S. cerevisiae* (ScDcp2), hDcp2 and SpDcp2. The positions of amino acids corresponding to the sequence of the vaccinia virus D10 protein are indicated. Black boxes represent consensus amino acids in all five sequences, whereas grey boxes highlight conserved amino acids. The Nudix motif consensus sequence is presented below the alignment. (**B**) Predicted three-dimensional structure of the active site of the vaccinia virus D10p (amino acids 111–123). The characteristic loop–α-helix–loop fold found in other decapping enzymes is shown in a darker shade of grey. (**C**) Mechanistic model for the two-metal-ion mechanism of the D10p decapping activity. In the chemical step, Glu^{132} and Glu^{145} are engaged in the co-ordination of bivalent cations, whereas Glu^{141} would be required for the polarization of the attacking water molecule involved in catalysis.

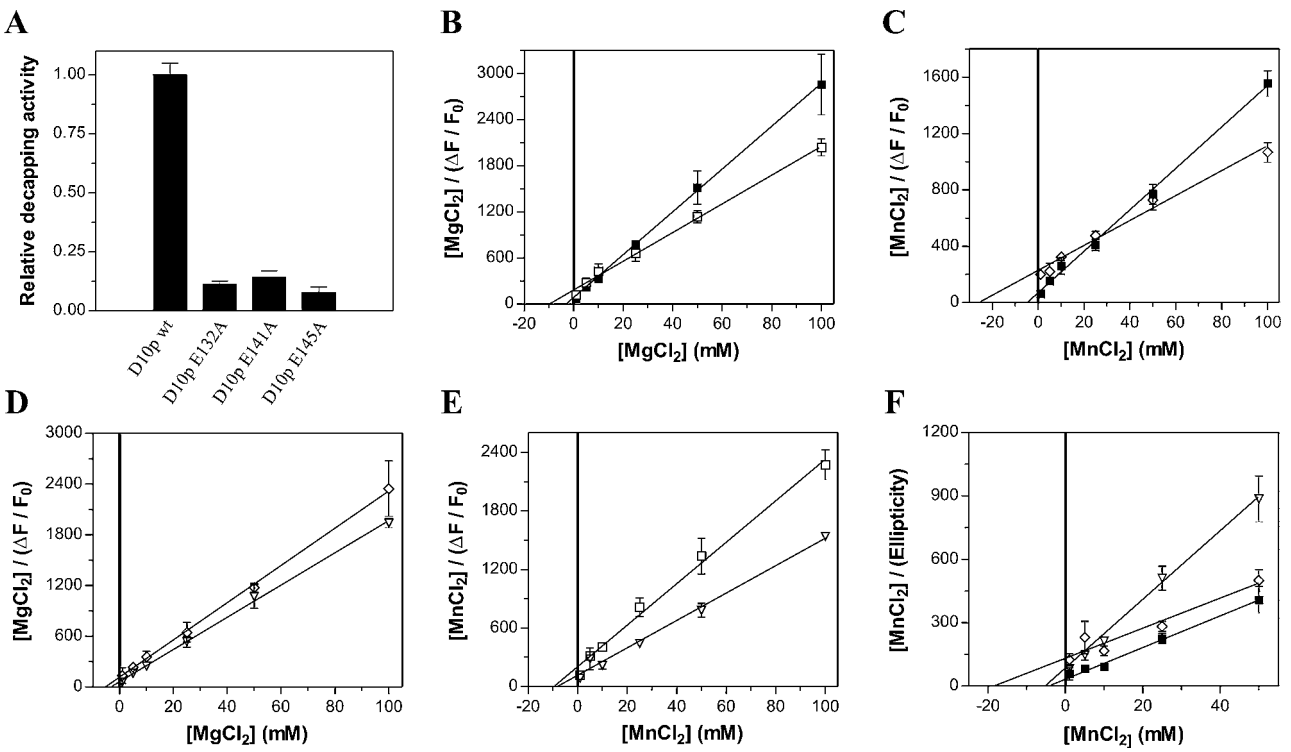

Figure 5 Effect of D10p glutamate mutants on activity and ion interaction

(**A**) The wild-type (wt) and D10p mutants (E132A, E141A and E145A) were incubated with a capped RNA substrate (0.5 μM) for 1.5 h at 37 °C with 10 mM $MgCl_2$ and 10 mM $MnCl_2$ in decapping buffer. The reactions were stopped by the addition of EDTA to 50 mM. The products were analysed by TLC, quantified by autoradiography, and are presented as a percentage of the wild-type activity. (**B**–**E**) Hanes–Wolf representation of the saturation isotherms of the fluorescence emission spectra for the binding of Mg^{2+} (**B** and **D**) and Mn^{2+} ions (**C** and **E**) to the wild-type D10p (■) and mutant D10p: E132A (□), E141A (▽) and E145A (◇). (**F**) Hanes–Wolf representation of the saturation isotherms of the CD far-UV spectra for the Mn^{2+} ion binding by wild-type D10p (■) and mutant D10p: E141A (▽) and E145A (◇).

we also observed that the D10p Nudix motif presents a very high conservation with the Nudix motif from the Dcp2p of other species (Figure 4A). Even though D10p has a low overall identity with the decapping enzymes presented in Figure 4(A), with values ranging from 18 % for hDcp2p and 22 % for the AtDcp2p, structural alignment of part of the Nudix domain of D10p with SpDcp2p showed a high level of homology between the catalytic centres of both enzymes. Amino acids 111–123 of D10p were therefore modelled based on the crystal structure of SpDcp2p (Figure 4B). The loop–α-helix–loop structural motif is conserved in D10p, along with the three critical glutamate residues (Glu^{141}, Glu^{144} and Glu^{145}) of the Nudix motif.

On the basis of this structural model, sequence alignments and previously suggested mechanisms [4,12,27], a model of the catalytic step of the decapping mechanism of D10p was produced (Figure 4C). In this model, a two-metal-ion mechanism is proposed for the chemical step of the reaction, where Glu^{141} is involved in polarization and positioning of a water molecule for the attack on the α–β-phosphate bond, whereas Glu^{132} and Glu^{145} both co-ordinate a bivalent cation. The Glu^{145}-co-ordinated ion ($Me^{2+}{}_1$) would assume a role in stabilizing the water for catalysis, whereas the Glu^{132}-co-ordinated ion ($Me^{2+}{}_2$) would sustain a structural role by stabilizing the interaction with RNA.

Mutational analysis

In order to provide experimental evidence for the proposed mechanism, we generated a series of enzymatic mutants. Glu^{132}, Glu^{141} and Glu^{145} were replaced by alanine, and the mutant polypeptides were expressed and purified in parallel with the wild-type enzyme. The relative activity of the purified mutants was assessed and compared with the wild-type D10p. Activity levels of 7.8 ± 0.2, 10.0 ± 1.0 and 12.2 ± 2.0 % were obtained for the E132A, E141A and E145A mutants respectively (Figure 5A). Furthermore, fluorescence spectroscopy was used to evaluate the ability of the mutants to bind Mg^{2+} and Mn^{2+} ions, in order to investigate a possible correlation between the lack of activity of the mutants and a decrease in their affinity for ions (Figures 5B–5E and Table 1). The E132A mutant showed a 5-fold reduced affinity for Mg^{2+}, but retained a Mn^{2+} affinity similar to that of the wild-type. The E141A mutant demonstrated only slight variations in both Mg^{2+} and Mn^{2+} binding, as is evident from the K_d and ΔG values. Finally, the E145A mutant also presented a slight 2-fold variation in its affinity for Mg^{2+}, whereas the Mn^{2+} binding was reduced 6-fold. In the case of the E132A and E145A mutants, only one proposed metal-ion-binding site was tentatively disrupted by the single point mutations, leaving a second possible binding site available for interaction. This probably explains the low variation obtained for the dissociation constants. The interaction of Mn^{2+} with the D10p E141A and E145A mutants was also confirmed using CD. The dissociation constants obtained are similar to those measured using fluorescence spectroscopy, with values of 6.4 ± 2.3 and 18.5 ± 5.8 mM for the titration of D10p E141A and E145A with Mn^{2+} ions respectively (Figure 5F). These results demonstrate that the mutations affect the binding of bivalent cations by the enzyme in ways that correlate with our proposed mechanism. It also points out a preference for Mg^{2+} at the Glu^{132} binding site, and a preference for Mn^{2+} at the Glu^{145} binding site.

DISCUSSION

To date, vaccinia virus represents the only mammalian virus for which decapping enzymes have been experimentally demonstrated [8–10]. The decapping activity appears to be critical to accelerate viral mRNA turnover and to eliminate competing cellular mRNAs. In the present study, the interaction of the vaccinia virus D10 decapping enzyme with bivalent cations was evaluated. According to our results, a synergistic activation of the D10p catalytic activity is observed when both Mg^{2+} and Mn^{2+} ions are present. Moreover, competitive alternative ligand-binding assays confirmed the presence of two metal-ion-binding sites on the enzyme. Our mutational analysis also revealed a preference by specific amino acids for a particular ion. Namely, we observed a decrease in Mg^{2+} ion binding when Glu^{132} was replaced by alanine and a reduced affinity for Mn^{2+} ions for the E145A mutant. These results support a two-metal-ion mechanism with the enzyme being able to catalyse its hydrolytic reaction in the presence of either bivalent ions, but with a higher activity when both sites are filled with their preferential ion. In our model, one of the metal ions ($Me^{2+}{}_2$) is co-ordinated by Glu^{132} and is involved in contacts with the β- and γ-phosphates of the cap, stabilizing the ^{m7}GDP leaving group, and probably involved in the positioning of the methylated cap for the hydrolytic attack. The other metal ion ($Me^{2+}{}_1$) is co-ordinated mainly by Glu^{145} and is likely to be required for the orientation of the water molecule for the attack on the α–β-pyrophosphate bond of the cap structure. Glu^{141} is also likely to be at hydrogen-bonding distance of $Me^{2+}{}_1$ and could be involved in its co-ordination, especially after the catalytic step, as seen in other Nudix hydrolases [12]. During the catalytic step, Glu^{141} would serve as a general base to either initiate catalysis or stabilize the attacking water molecule [12].

The mechanism described here for the D10 viral decapping enzyme could apply to other decapping enzymes in metazoans. However, analysis of the D10p sequence showed only partial homology with Dcp2 proteins. Although the Nudix motif is absolutely conserved, the Boxes A and B commonly found in Dcp2p are virtually absent from D10p. The protein, with its 248 amino acids, is also much shorter than the *S. pombe*, *S. cerevisiae*, *A. thaliana* and human Dcp2 proteins [6,28]. Nonetheless, the catalytic core of D10p seems to share common features with the one found in Dcp2 proteins. For instance, the AtDcp2 protein has been shown to lack the particular F^- ion susceptibility which is characteristic of some members of the Nudix hydrolases family, a property that appeared to be shared by D10p [4,13]. Furthermore, modelling of the active site of D10p on the SpDcp2p structure outlined a high homology of the catalytic centre of these enzymes. Although experimental evidence is lacking, a two-metal-ion mechanism has also been postulated for AtDcp2p [3]. Therefore we hypothesize that the two-metal-ion mechanism of the vaccinia virus decapping enzyme might be common to other Dcp2 proteins. Supporting evidence comes from the characterization of the hDcp2p, SpDcp2p and AtDcp2p [3,4,29]. In all cases, the enzymes were active in the presence of Mg^{2+}, but the addition of Mn^{2+} yielded a major increase in decapping activity, similarly to what was observed for D10p. Glu^{132}, proposed here to be involved in the co-ordination of a metal ion, is invariably conserved in all Dcp2-like enzymes examined so far, and has been shown in some Nudix family members to be required for activity [16,30]. Previous studies on decapping enzymes did, however, suggest another glutamate residue for ion co-ordination [6,31]. Glu^{192} in *S. pombe* was observed to be pointing towards the bound ATP in the resolved crystal structure. This residue is found in many decapping enzymes, but is not conserved in D10p [6,32]. Since this glutamate residue is critical for decapping activity in *S. pombe*, it might be involved in substrate recognition, co-ordination of the second metal ion, or the possible co-ordination of a third metal ion [6,31]. Future work on decapping enzymes will tell us whether the two-metal-ion mechanism utilized by D10p is also employed by Dcp2 proteins or is only shared with other poxvirus decapping enzymes.

Another interesting feature of the vaccinia virus D10p is its lack of an obvious cofactor for its decapping activity [8]. Dcp2 proteins typically form heterodimers with Dcp1 proteins, which possess no intrinsic decapping activity and, although not required for Dcp2 activity in humans and plants, seem to act in stabilizing the most catalytically efficient conformation of Dcp2p [3,4,31]. Moreover, structural analysis revealed DcpS to be a dimeric protein [33]. Interestingly, D10p was only present as a monomer *in vitro* (results not shown). However, it cannot be excluded that the protein could have other interaction partners in cells. The vaccinia virus possesses a second decapping enzyme encoded by the D9 gene. Unlike the Dcp1 protein of humans and yeasts, D9p demonstrates an effective hydrolytic decapping activity of its own [8,10]. Even though D9p is expressed during early transcription of the virus, whereas D10p is under the regulation of a late promoter, they might interact during their overlapping lifespans to modulate the decapping efficiency of one or both of the enzymes. It would be equally interesting to investigate the possible interaction of D10p with the cellular Dcp1p. Even if the amino acids of the mapped interface of Dcp2p with Dcp1p are not conserved in D10p, with the presence of only one of the eight amino acids outlined for recognition, a different interaction may be possible to either affect D10p activity or its localization in cells [31]. Moreover, the Ge-1 cellular protein could be investigated for possible interactions with D10p since it has been shown to localize to the P-bodies and interact with host Dcp enzymes [34–36]. Further analysis could lead to the discovery of cellular interaction partners with D10p and assess its possible localization to the mRNA processing bodies in infected cells.

ACKNOWLEDGEMENTS

We thank Dr Guy Lemay (Université de Montréal) for the gift of the vaccinia virus DNA.

FUNDING

This work was supported by a grant from the Canadian Institutes for Health Research [grant number MOP-62710]. M. B. is a New Investigator Scholar from the Canadian Institutes for Health Research. J. P. P. holds the Canada Research Chair in Genomics and Catalytic RNA. The RNA group is supported by a grant from the Canadian Institutes for Health Research and by the Université de Sherbrooke. Both M. B. and J. P. P. are members of the Infectious Diseases Group of the Centre de Recherche Clinique Étienne-Lebel.

REFERENCES

1 Wickens, M. and Goldstrohm, A. (2003) A place to die, a place to sleep. Science **300**, 753–755
2 Sheth, U. and Parker, R. (2003) Decapping and decay of messenger RNA occur in cytoplasmic processing bodies. Science **300**, 805–808
3 Wang, Z., Jiao, X., Carr-Schmid, A. and Kiledjian, M. (2002) The hDcp2 protein is a mammalian mRNA decapping enzyme. Proc. Natl. Acad. Sci. U.S.A. **99**, 12663–12668
4 Gunawardana, D., Cheng, H. C. and Gayler, K. R. (2008) Identification of functional domains in *Arabidopsis thaliana* mRNA decapping enzyme (AtDcp2) Nucleic Acids Res. **36**, 203–216
5 Steiger, M., Carr-Schmid, A., Schwartz, D. C., Kiledjian, M. and Parker, R. (2003) Analysis of recombinant yeast decapping enzyme. RNA **9**, 231–238
6 She, M., Decker, C. J., Chen, N., Tumati, S., Parker, R. and Song, H. (2006) Crystal structure and functional analysis of Dcp2p from *Schizosaccharomyces pombe*. Nat. Struct. Mol. Biol. **13**, 63–70
7 Liu, H., Rodgers, N. D., Jiao, X. and Kiledjian, M. (2002) The scavenger mRNA decapping enzyme DcpS is a member of the HIT family of pyrophosphatases. EMBO J. **21**, 4699–4708

8 Parrish, S., Resch, W. and Moss, B. (2007) Vaccinia virus D10 protein has mRNA decapping activity, providing a mechanism for control of host and viral gene expression. Proc. Natl. Acad. Sci. U.S.A. **104**, 2139–2144

9 Parrish, S. and Moss, B. (2006) Characterization of a vaccinia virus mutant with a deletion of the D10R gene encoding a putative negative regulator of gene expression. J. Virol. **80**, 553–561

10 Parrish, S. and Moss, B. (2007) Characterization of a second vaccinia virus mRNA-decapping enzyme conserved in poxviruses. J. Virol. **81**, 12973–12978

11 Shors, T., Keck, J. G. and Moss, B. (1999) Down regulation of gene expression by the vaccinia virus D10 protein. J. Virol. **73**, 791–796

12 Mildvan, A. S., Xia, Z., Azurmendi, H. F., Saraswat, V., Legler, P. M., Massiah, M. A., Gabelli, S. B., Bianchet, M. A., Kang, L. W. and Amzel, L. M. (2005) Structures and mechanisms of Nudix hydrolases. Arch. Biochem. Biophys. **433**, 129–143

13 McLennan, A. G. (2006) The Nudix hydrolase superfamily. Cell. Mol. Life Sci. **63**, 123–143

14 Dunckley, T. and Parker, R. (1999) The DCP2 protein is required for mRNA decapping in *Saccharomyces cerevisiae* and contains a functional MutT motif. EMBO J. **18**, 5411–5422

15 Liu, H. and Kiledjian, M. (2006) Decapping the message: a beginning or an end. Biochem. Soc. Trans. **34**, 35–38

16 Ooga, T., Yoshiba, S., Nakagawa, N., Kuramitsu, S. and Masui, R. (2005) Molecular mechanism of the *Thermus thermophilus* ADP-ribose pyrophosphatase from mutational and kinetic studies. Biochemistry **44**, 9320–9329

17 Legler, P. M., Massiah, M. A. and Mildvan, A. S. (2002) Mutational, kinetic, and NMR studies of the mechanism of *E. coli* GDP-mannose mannosyl hydrolase, an unusual Nudix enzyme. Biochemistry **41**, 10834–10848

18 Conyers, G. B., Wu, G., Bessman, M. J. and Mildvan, A. S. (2000) Metal requirements of a diadenosine pyrophosphatase from *Bartonella bacilliformis*: magnetic resonance and kinetic studies of the role of Mn^{2+}. Biochemistry **39**, 2347–2354

19 Gabelli, S. B., Bianchet, M. A., Ohnishi, Y., Ichikawa, Y., Bessman, M. J. and Amzel, L. M. (2002) Mechanism of the *Escherichia coli* ADP-ribose pyrophosphatase, a Nudix hydrolase. Biochemistry **41**, 9279–9285

20 Painter, G. R., Wright, L. L., Hopkins, S. and Furman, P. A. (1991) Initial binding of 2′-deoxynucleoside 5′-triphosphates to human immunodeficiency virus type 1 reverse transcriptase. J. Biol. Chem. **266**, 19362–19368

21 Schwede, T., Kopp, J., Guex, N. and Peitsch, M. C. (2003) SWISS-MODEL: an automated protein homology-modeling server. Nucleic Acids Res. **31**, 3381–3385

22 Guranowski, A. (1990) Fluoride is a strong and specific inhibitor of (asymmetrical) Ap4A hydrolases. FEBS Lett. **262**, 205–208

23 Painter, G. R., Wright, L. L., Hopkins, S. and Furman, P. A. (1991) Initial binding of 2′-deoxynucleoside 5′-triphosphates to human immunodeficiency virus type 1 reverse transcriptase. J. Biol. Chem. **266**, 19362–19368

24 Bougie, I., Charpentier, S. and Bisaillon, M. (2003) Characterization of the metal ion binding properties of the hepatitis C virus RNA polymerase. J. Biol. Chem. **278**, 3868–3875

25 Martins, A. and Shuman, S. (2003) Mapping the triphosphatase active site of baculovirus mRNA capping enzyme LEF4 and evidence for a two-metal mechanism. Nucleic Acids Res. **31**, 1455–1463

26 Gong, C., Martins, A. and Shuman, S. (2003) Structure–function analysis of *Trypanosoma brucei* RNA triphosphatase and evidence for a two-metal mechanism. J. Biol. Chem. **278**, 50843–50852

27 Steitz, T. A. and Steitz, J. A. (1993) A general two-metal-ion mechanism for catalytic RNA. Proc. Natl. Acad. Sci. U.S.A. **90**, 6498–6502

28 Iwasaki, S., Takeda, A., Motose, H. and Watanabe, Y. (2007) Characterization of *Arabidopsis* decapping proteins AtDCP1 and AtDCP2, which are essential for post-embryonic development. FEBS Lett. **581**, 2455–2459

29 Steiger, M., Carr-Schmid, A., Schwartz, D. C., Kiledjian, M. and Parker, R. (2003) Analysis of recombinant yeast decapping enzyme. RNA **9**, 231–238

30 Mishima, M., Sakai, Y., Itoh, N., Kamiya, H., Furuichi, M., Takahashi, M., Yamagata, Y., Iwai, S., Nakabeppu, Y. and Shirakawa, M. (2004) Structure of human MTH1, a Nudix family hydrolase that selectively degrades oxidized purine nucleoside triphosphates. J. Biol. Chem. **279**, 33806–33815

31 She, M., Decker, C. J., Svergun, D. I., Round, A., Chen, N., Muhlrad, D., Parker, R. and Song, H. (2008) Structural basis of Dcp2 recognition and activation by Dcp1. Mol. Cell **29**, 337–349

32 van Dijk, E., Cougot, N., Meyer, S., Babajko, S., Wahle, E. and Séraphin, B. (2002) Human Dcp2: a catalytically active mRNA decapping enzyme located in specific cytoplasmic structures. EMBO J. **21**, 6915–6924

33 Liu, S. W., Rajagopal, V., Patel, S. S. and Kiledjian, M. (2008) Mechanistic and kinetic analysis of the DcpS scavenger decapping enzyme. J. Biol. Chem. **283**, 16427–16436

34 Xu, J., Yang, J. Y., Niu, Q. W. and Chua, N. H. (2006) *Arabidopsis* DCP2, DCP1, and VARICOSE form a decapping complex required for postembryonic development. Plant Cell **18**, 3386–3398

35 Fenger-Grøn, M., Fillman, C., Norrild, B. and Lykke-Andersen, J. (2005) Multiple processing body factors and the ARE binding protein TTP activate mRNA decapping. Mol. Cell **20**, 905–915

36 Yu, J. H., Yang, W. H., Gulick, T., Bloch, K. D. and Bloch, D. B. (2005) Ge-1 is a central component of the mammalian cytoplasmic mRNA processing body. RNA **11**, 1795–1802

Received 26 November 2008/29 January 2009; accepted 11 February 2009
Published as BJ Immediate Publication 11 February 2009, doi:10.1042/BJ20082296

Biochem. J. (2009) **420**, 27–35 (Printed in Great Britain) doi:10.1042/BJ20082296

online data

SUPPLEMENTARY ONLINE DATA

Characterization of the vaccinia virus D10 decapping enzyme provides evidence for a two-metal-ion mechanism

Marie F. SOULIÈRE, Jean-Pierre PERREAULT and Martin BISAILLON[1]

RNA Group/Groupe ARN, Département de Biochimie, Faculté de Médecine et des Sciences de la Santé, Université de Sherbrooke, Sherbrooke, QC, Canada, J1H 5N4

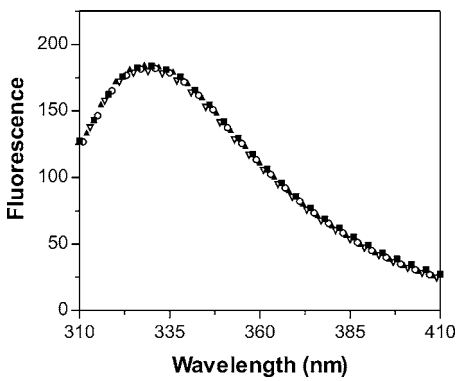

Figure S1 Specificity of metal ion binding to D10p

Fluorescence emission spectra of 1 μM D10p in decapping buffer. Excitation was performed at 290 nm, and the emission spectrum was scanned from 310 to 440 nm. The fluorescence emission of D10p is monitored in the absence (■) or in the presence of 50 mM Ca^{2+} (○), Na^{+} (▲) or Li^{+} (▽) ions.

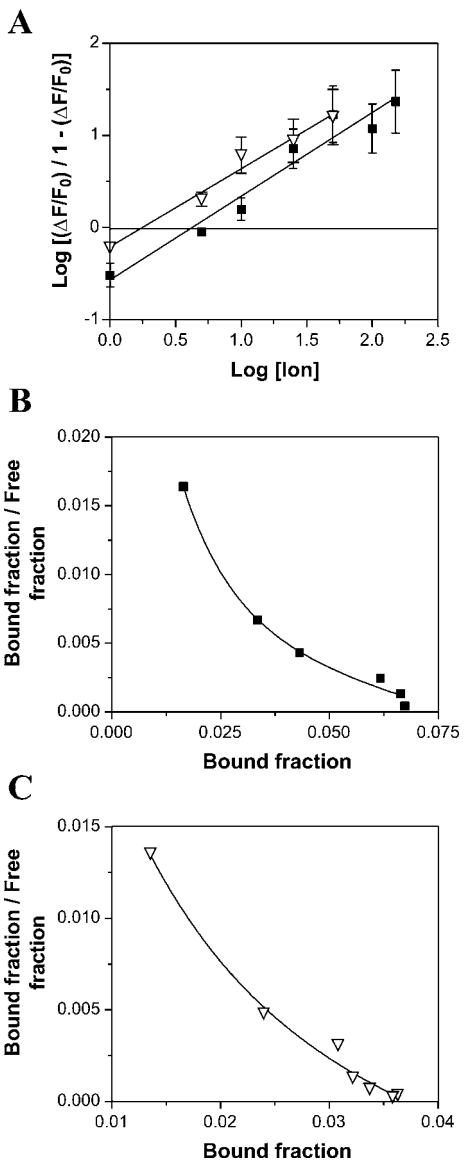

Figure S2 Hill and Scatchard derivations for metal ion binding to D10p

Derivation of the binding data from fluorescence spectroscopy binding experiments with the Hill or Scatchard equations. (**A**) Hill plots for Mn^{2+} (■) and Mg^{2+} (▽) binding to D10p, and Scatchard plots for the interaction of Mn^{2+} (**B**) and Mg^{2+} (**C**) with the enzyme.

[1] To whom correspondence should be addressed (email Martin.Bisaillon@USherbrooke.ca).

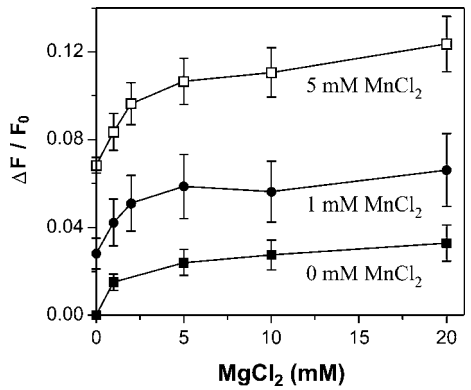

Figure S3 Competitive alternative ligand-binding experiment

Standard titration assays were performed using Mg^{2+} ions in the presence of increasing amounts of Mn^{2+} ions. The concentrations of Mn^{2+} ions used in these experiments were 0 (■), 1 (●) and 5 (□) mM.

Received 26 November 2008/29 January 2009; accepted 11 February 2009
Published as BJ Immediate Publication 11 February 2009, doi:10.1042/BJ20082296